Naval Research Laboratory

Washington, DC 20375-5320

Preconcentration for Improved Long-Term Monitoring of Contaminants in Groundwater: Sorbent Development

Brandy J. White
Brian J. Melde
Paul T. Charles

Center for Bio/Molecular Science and Engineering

February 11, 2013

REPORT DOCUMENTATION PAGE

Public reporting burden for this collection of information is estimated to average 1 hour per response, including the time for reviewing instructions, searching existing data sources, gathering and maintaining the data needed, and completing and reviewing this collection of information. Send comments regarding this burden estimate or any other aspect of this collection of information, including suggestions for reducing this burden to Department of Defense, Washington Headquarters Services, Directorate for Information Operations and Reports (0704-0188), 1215 Jefferson Davis Highway, Suite 1204, Arlington, VA 22202-4302. Respondents should be aware that notwithstanding any other provision of law, no person shall be subject to any penalty for failing to comply with a collection of information if it does not display a currently valid OMB control number. **PLEASE DO NOT RETURN YOUR FORM TO THE ABOVE ADDRESS.**

1. REPORT DATE *(DD-MM-YYYY)*	2. REPORT TYPE	3. DATES COVERED *(From - To)*
11-02-2013	Formal Report	01-02-2008 to 30-04-2012

4. TITLE AND SUBTITLE

Preconcentration for Improved Long-Term Monitoring of Contaminants in Groundwater: Sorbent Development

5a. CONTRACT NUMBER

5b. GRANT NUMBER

5c. PROGRAM ELEMENT NUMBER

6. AUTHOR(S)

Brandy J. White, Brian J. Melde, and Paul T. Charles

5d. PROJECT NUMBER
ER-1604

5e. TASK NUMBER

5f. WORK UNIT NUMBER
69-9629

7. PERFORMING ORGANIZATION NAME(S) AND ADDRESS(ES)

Naval Research Laboratory
4555 Overlook Avenue, SW
Washington, DC 20375-5320

8. PERFORMING ORGANIZATION REPORT NUMBER

NRL/FR/6910--12-10,235

9. SPONSORING / MONITORING AGENCY NAME(S) AND ADDRESS(ES)

Strategic Environmental Research and Development Program
901 N. Stuart St., Suite 303
Arlington, VA 22203-1853

10. SPONSOR / MONITOR'S ACRONYM(S)

SERDP

11. SPONSOR / MONITOR'S REPORT NUMBER(S)

12. DISTRIBUTION / AVAILABILITY STATEMENT

Approved for public release; distribution is unlimited.

13. SUPPLEMENTARY NOTES

14. ABSTRACT

This report summarizes the results of studies directed at the development of organosilicate sorbents for the capture and preconcentration of nitroenergetics targets and perchlorates from natural water sources. Two distinct types of sorbents were developed. The first, directed at nitroenergetics, utilizes new approaches to target templating and a hierarchical structure. The second, directed at perchlorates, utilizes the hierarchical structure with alkylammonium surface modifications. Both materials provide semiselective target capture and offer advantages over commercially available products. Application of the sorbents in single and mixed target solutions is demonstrated. Nitroenergetic capture from natural water sources is also evaluated.

15. SUBJECT TERMS

TNT	Perchlorate	Preconcentration
Nitroenergetic	Sorbent	Detection

16. SECURITY CLASSIFICATION OF:

a. REPORT	b. ABSTRACT	c. THIS PAGE	17. LIMITATION OF ABSTRACT	18. NUMBER OF PAGES	19a. NAME OF RESPONSIBLE PERSON
Unclassified	Unclassified	Unclassified	Unlimited	43	Brandy J. White
					19b. TELEPHONE NUMBER *(include area code)* 202-404-6100

CONTENTS

FIGURES

TABLES

PRECONCENTRATION FOR IMPROVED LONG-TERM MONITORING OF CONTAMINANTS IN GROUNDWATER: SORBENT DEVELOPMENT

INTRODUCTION

The Center for Bio/Molecular Science and Engineering at the Naval Research Laboratory (NRL) initiated a program in February 2008 to develop new organosilicate sorbents for the preconcentration of nitroenergetic contaminants from natural water sources in order to enhance detection by portable instrumentation. The intention was to demonstrate that existing portable systems could be utilized for reliable monitoring of contaminant levels, providing alternatives to the costly processes involved in sampling for later analysis by a laboratory. The original effort focused on development and evaluation of materials including those based on new synthetic strategies and was directed at providing semiselective or class-selective capture of nitroenergetic targets from natural water sources. In 2009, the effort was expanded to include perchlorates as targets of interest and extended to include development of the systems necessary for use of the sorbent materials in a system applicable to long-term and/or remote monitoring of targets. This report focuses on the development and evaluation of materials applicable to preconcentration of targets. Development of the associated systems, ongoing at the time of this report, will be the topic of a future publication.

Background

In the United States there exist a number of sites contaminated with one or more compounds related to weapons technologies. Compounds such as nitroenergetics and perchlorates, components of common ordnance, are of particular interest. To mitigate threats to the environment and personnel at these sites and to comply with environmental regulations, it is necessary to conduct long-term monitoring of sites undergoing remediation, as well as sites that may eventually require cleanup. Monitoring these sites can present significant challenges. The rapid diffusion and migration of nitroenergetic compounds and their resulting dilution leads to low concentration levels in collected samples. Due to the low concentrations, matrix complexity, and strict reproducibility and reliability constraints, offsite analysis of samples is the standard for evaluating sites of interest [1]. This type of sample collection and analysis process is both expensive and time consuming. The methods utilize liquid or gas chromatography, techniques that do not lend themselves well to portable devices and methods. Portable methods are desirable as onsite indicators of the need for further testing and/or as in situ methods for continuous monitoring of contamination levels. These approaches are generally less time consuming and can be considerably less expensive than traditional methods. Unfortunately, many portable methods lack either the robustness, ease of use, quantitative capability, or sensitivity necessary for field application [2–5].

Electrochemical (EC) detection shows promise for onsite monitoring applications, offering the potential for low-cost, low-power solutions. Remote monitoring systems based on electrochemical measurements have been described [6]. Sensitivity to matrix components and interferents has limited the applicability of this technique. Another promising technology for field application as miniaturized sensors is ion mobility spectroscopy (IMS) [7,8]. Several hand-held instruments based on IMS are available [9]. The technology has also been applied to monitoring concentrations of contaminants in soils [10]. Current

applications are limited to compounds with higher vapor pressures or to samples that are preheated due to the need for samples to be gaseous.

Standardized methods developed for field applications typically rely on preconcentration of targets to achieve concentrations within the range of analysis [11,12]. This type of solid phase extraction (SPE) of targets offers the potential to address the shortfalls in both EC and IMS based detection. SPE involves adsorption of target onto a solid support. Desorption is accomplished through the use of a thermal process or through elution under particular conditions. The intent is to adsorb target from a large sample volume and desorb it into a small volume, leading to a higher target concentration. Organosilicate materials offer novel advantages to preconcentration approaches and provide the potential to address preconcentration needs for the targets of interest. The section below highlights the primary characteristics of these materials and previous studies relevant to the current effort.

Porous Organosilicate Materials

Periodic mesoporous organosilicates (PMOs) are organic–inorganic polymers with highly ordered pore networks and large internal surface areas (typically >1000 m^2/g). The alternating siloxane and organic moieties give PMOs properties associated with both organic and inorganic materials [13,14]. Siloxane groups provide the structural rigidity required for the pore templating process. In addition, the silica component of the PMOs provides a degree of hydrophilic character useful for applications in aqueous systems. Organic functional groups within the PMO offer those interactions with targets typically associated with organic polymers. Precursors containing different organic bridging groups have been used to produce a variety of PMOs with unique chemical properties. Experimental parameters, such as the selection of different precursors, surfactants, and functional silanes, allow the design of porous materials with structural and chemical properties optimized for a given application.

Fig. 1 shows a typical protocol for the synthesis of PMO materials. The surfactant is dissolved in acidified ethanol at a concentration exceeding the critical micelle concentration. When the micelles are established, the siloxane precursors are added. Following condensation, the surfactant is extracted, leaving an open porous structure with the organization resulting from the original micelles. The organization of the pores of a PMO is directed by the surfactant micelles. A surfactant commonly employed in the synthesis outlined in Fig. 1 is Brij®76 (polyoxyethylene (10) stearyl ether, $C_{18}H_{37}(OCH_2CH_2)_nOH$, n~10). This is an alkylene oxide surfactant that provides, in general, pore sizes of about 30 Å under standard conditions [15–17]. Various arrangements of micelles (hexagonal, lamellar, etc.) are possible depending on the choice of surfactant, acid, temperature, and concentration. Recent advances provide the potential for hierarchical structures in this type of material. Hierarchical sorbents typically use a larger surfactant (Pluronic P123, for example) combined with a swelling agent during synthesis. Spinodal decomposition results in phase separations that produce macroscale structure containing ordered mesoporous domains [18–20]. Macropores provide improved diffusion throughout the sorbent material and enhanced access to the mesopore volume.

Fig. 1 — Typical synthesis for periodic mesoporous organosilicates (PMOs)

Prior to the beginning of this effort, we had demonstrated that PMOs could be engineered to provide semiselective sorbents for nitroenergetic compounds [16,21]. The early materials provided limited selectivity and demonstrated high backpressures when applied in column formats. The study described here sought to overcome those limitations and demonstrate the potential for preconcentration by organosilicate sorbents. Over the course of the study, several advances were made in the design of the sorbent materials. (1) Co-condensation of sorbents was found to provide a compromise between desirable morphological characteristics and necessary binding characteristics. (2) New imprint templates were developed leading to a more effective imprinting approach. (3) Lessons learned for PMO sorbents were applied to the development of hierarchical sorbents to alleviate backpressure when used in column formats. In addition, novel sorbents directed at capture of perchlorates were developed based on hierarchical structures and grafted functional groups. These advances and approaches are detailed in this report.

APPROACH

Reagents

Sodium perchlorate, sodium perrhenate, ammonium nitrate, ammonium thiocyanate, ammonium sulfate, ammonium phosphate, p-cresol (pCr), and p-nitrophenol (pNP) were purchased from Sigma-Aldrich (St. Louis, MO). 2,4,6-Trinitrotoluene (TNT), hexahydro-1,3,5-trinitro-1,3,5-triazine (RDX), nitroglycerin (NG), octahydro-1,3,5,7-tetranitro-1,3,5,7-tetrazocane (HMX), and 2,4-dinitrotoluene (DNT) were purchased from Cerilliant (Round Rock, TX). Chemicals were used as received. Chemicals used for synthesis of materials are detailed in Table 1. Purolite® A530E and A532E, strong base anion exchange resins, were gifts from Purolite (Bala Cynwyd, PA). Water was deionized to 18.2 MΩ cm using a Millipore Milli Q UV-Plus water purification system. Artificial sea water was prepared using sea salts as directed by the supplier (Sigma-Aldrich). Pond water samples were collected from a park in Alexandria, Virginia. Groundwater was collected from wells in Hanover, New Hampshire, and Fulton, Maryland (depth of 213 m). Soil samples were collected from munitions testing sites on Holloman Air Force Base, Alamogordo, New Mexico, and analyzed using Environmental Protection Agency (EPA) Method 8330B by the Cold Regions Research and Engineering Laboratory, Engineer Research and Development Center, U.S. Army Corps of Engineers, Hanover, New Hampshire.

Table 1 — Synthesis Reagents

Compound	Abbrev	Supplier	Function	Notes
Nitroenergetic Target Directed Materials				
Bis(trimethoxysilylethyl)benzene	DEB	Gelest	Precursor	
Phenyltrimethoxysilane	PTS	Gelest	Precursor	
1,2-Bis(trimethoxysilyl)ethane	BTE	Gelest	Precursor	
Hydrochloric acid	HCl	Sigma-Aldrich	Solvent System	
Polyoxyethylene (10) stearyl ether, $C_{18}H_{37}(OCH_2CH_2)_nOH$, n~10	Brij®76	Sigma-Aldrich	Surfactant	
3,5-Dinitrobenzoyl chloride		Sigma-Aldrich	Target Analog	98%
Dichloromethane		Sigma-Aldrich	Template Synthesis	Solvent >99.5%
Sodium bicarbonate	$NaHCO_3$	Sigma-Aldrich	Template Synthesis	Purification
Magnesium turnings		Sigma-Aldrich	Phase Separation	98%
Ionic Target Directed Materials				
N-trimethoxysilylpropyl-N, N, N-trimethylammonium chloride	TSPMC, M	Gelest	Grafted Group	50% in methanol
N-trimethoxysilylpropyl-N, N, N-tri-n-butylammonium chloride	TSPBC, B	Gelest	Grafted Group	50% methanol
Tetramethyl orthosilicate	TMOS	Sigma-Aldrich	Precursor	98%
Toluene		Sigma-Aldrich	Grafting	Solvent
Used in Materials for Both Targets				
1,3,5-trimethylbenzene	TMB	Sigma-Aldrich	Spinodal Decomposition	Mesitylene
Poly(ethylene glycol)-*block*-poly(propylene glycol)-*block*-poly(ethylene glycol) average M_n~5800	P123	BASF	Surfactant	Pluronic P123
Nitric acid	HNO_3	Sigma-Aldrich	Solvent System	
Ethanol		Warner-Graham	Solvent System	200 proof

Material Synthesis

Two major variations on material synthesis were utilized for nitroenergetic targets during the course of these studies. Here, we describe in general terms the approaches used. For detailed synthetic processes, please refer to the cited papers.

PMO Synthesis

Fig. 1 presents the basic steps in synthesis of a PMO material [22,23]. In general, the Brij®76 surfactant was dissolved in an aqueous solution of HCl with or without the appropriate imprint template. The precursor or precursor mixture was added to the solution dropwise, and the mixture was heated overnight. Product was collected by vacuum filtration, and the surfactant was extracted by refluxing aqueous HCl.

The target analog used for imprinting the PMOs (Fig. 2) was generated through esterification of Brij®76 with 3,5-dinitrobenzoyl chloride [24–26]. Briefly, Brij®76 (2 g; 2.81 mmol) and 3,5-dinitrobenzoyl chloride (1.3 g; 6 mmol) were dissolved in 60 mL of dichloromethane. Magnesium turnings were added and the mixture was refluxed for 2 h. The liquid was shaken with 60 mL 2% $NaHCO_3$ in a separatory funnel. The organic phase was then extracted and evaporated under vacuum. The resulting dinitrobenzene (DNB)-modified Brij®76 was orange in color [15,17,27].
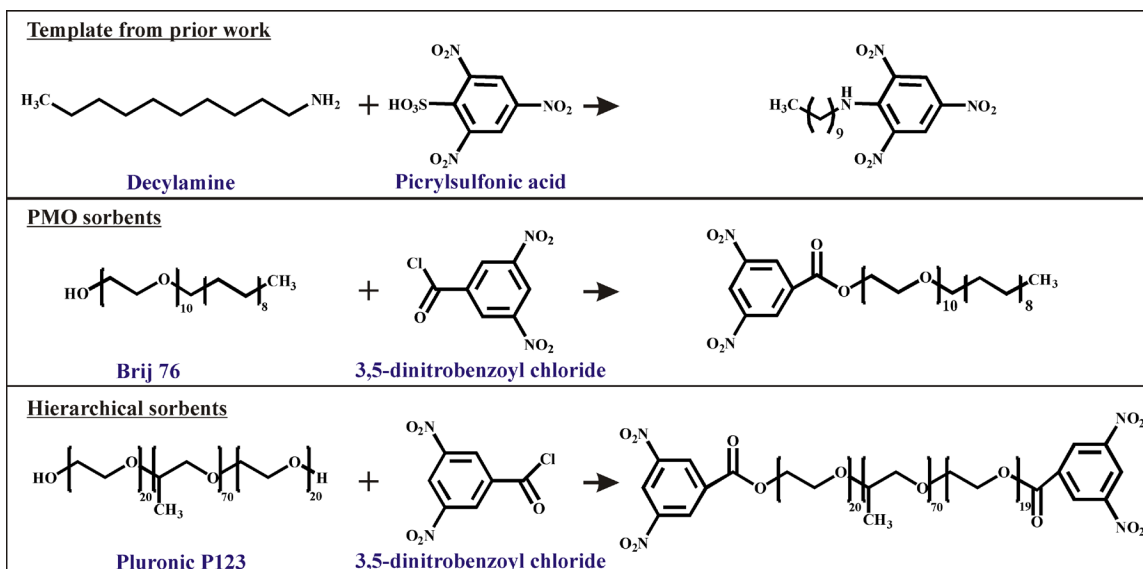
Fig. 2 — Target analogs (or imprint templates) used for prior work with organosilicate sorbents (top), the PMO materials described here (center), and the hierarchical sorbents described here (bottom)

Hierarchical Sorbent Synthesis

Synthesis of the hierarchical materials was accomplished using a variation of the technique described above [15,28]. Pluronic P123 surfactant was dissolved with mesitylene and with or without the appropriate template in aqueous nitric acid. The precursor or precursor mixture was added dropwise to the

solution, forming a white gel. Following curing, the product was refluxed in acidified ethanol to remove the surfactant, and product was collected by vacuum filtration.

The target analog for imprinting the hierarchical materials (Fig. 2) was prepared by esterification of Pluronic P123 with 3,5-dinitrobenzoyl chloride. This was accomplished as follows: 8 g P123, 1.27 g 3,5-dinitrobenzoyl chloride, and magnesium turnings were added to 60 mL dichloromethane and refluxed for 2 h. The solution was shaken with 60 mL 2% aqueous $NaHCO_3$. The organic phase was collected and evaporated to yield the yellow, modified surfactant [29–31].

For materials directed at capture of perchlorates, a similar approach was taken to synthesis of a scaffold. The materials were synthesized based on a previously published approach [18,32]. Pluronic P123 and mesitylene were dissolved in HNO_3 with magnetic stirring and heating. The stirring mixture was allowed to cool to room temperature and TMOS was added dropwise. The mixture was stirred until homogeneous, transferred to a culture tube or a Teflon jar container, sealed tightly, and heated overnight. The white monolith was dried in the unsealed container for approximately 5 d. Surfactant was removed by calcination under ambient atmosphere. Materials were dried at 110 °C prior to grafting with alkylammonium silanes. Grafting of alkylammonium groups was accomplished using materials thoroughly dried at 110 °C. Sorbent material was added to toluene followed by addition of a designated amount of TSPMC and/or TSPBC. The mixture was refluxed for 24 h. Grafted product was collected by vacuum filtration, washed with toluene and ethanol, and dried at 110 °C. The nomenclature of functionalized materials reflects the amounts of TSPMC and/or TSPBC used in the grafting procedure. For example, material designated HX1M3B was prepared by refluxing 1 g of HX with 1 mmol of TSPMC (M) and 3 mmol of TSPBC (B).

Material Characterization

A Micromeritics accelerated surface area and porosimetry analyzer (ASAP 2010) was used for N_2 sorption experiments performed at 77 K. Prior to analysis, samples were degassed to 1 μm Hg at 100 ºC. Standard methods were applied to the calculation of characteristics. Surface area was determined by use of the Brunauer-Emmett-Teller (BET) method; pore size was calculated by the Barrett-Joyner-Halenda (BJH) method from the adsorption branch of the isotherm; total pore volume was calculated by the single point method at relative pressure (P/P_0) 0.97. Thermogravimetric analysis was performed using a TA Instruments Hi-Res 2950 Thermogravimetric Analyzer under a N_2 atmosphere; temperature was ramped 5 ºC/min to 800 ºC. Powder X-ray diffraction (XRD) patterns were obtained with one of two systems: (1) a Rigaku high-resolution powder diffractometer with 18 kW CuKα radiation derived from a high-power Rigaku rotating anode X-ray generator or (2) CuKα radiation from a Brüker MICROSTAR-H X-ray generator operated at 40 kV and 30 mA equipped with a 3 mRadian collimator, and a Brüker Platinum-135 CCD area detector (room temperature). A custom fabricated beamstop was mounted on the detector to allow data collection to approximately 0.4° 2θ (approximately 210 Å) with a sample-to-detector distance of 30 cm. After unwarping the images, the XRD[2] plug-in was used to integrate the diffraction patterns from 0.6° to 8° 2θ.

Conducting carbon tape was used to mount samples on stubs for imaging by scanning electron microscopy (SEM). Sputter coating with gold under argon was accomplished using a Cressington 108 auto sputter coater (duration 60 sec). Scanning electron micrographs of the samples were collected using a LEO 1455 SEM (Carl Zeiss SMT, Inc., Peabody, MA). For imaging via transmission electron microscopy (TEM), samples were deposited onto a holey carbon grid (200 mesh copper, SPI, West Chester, PA) and viewed under an energy filtering transmission electron microscope (LIBRA 120 EFTEM, Carl Zeiss SMT, Peabody, MA) operated at 120 kV. Zero loss, brightfield, energy filtered (EF) TEM images were captured on a bottom-mounted digital camera (KeenView, Olympus SIS, Montvale, NJ).

Experimental Setup

Analysis of samples containing nitroenergetic targets was carried out on a Shimadzu high performance liquid chromatography (HPLC) system with dual-plunger parallel flow solvent delivery modules (LC-20AD) and an auto-sampler (SIL-20AC) coupled to a photodiode array detector (SPD-M20A). A modification of EPA Method 8330 was employed. The stationary phase was a 250 × 4.6 mm Altech Alltima C18 (5 μm) analytical column; an isocratic 50:50 methanol:water mobile phase was employed. A 100 μL sample injection was used with a flow rate of 1.3 mL/min. UV/vis detection of targets was accomplished at 254 nm with the exception of nitroglycerin which was detected at 214 nm. This method gives reliable detection at 8 ppb for the targets considered. Eight-point target calibration curves were used with all experiments to verify method performance, and stock target concentrations were measured as a reference for each experiment. The variation in the calibration curves was ±5%.

Ion chromatography (IC) was used for analysis of perchlorate and other ionic targets. Analysis was carried out on a Dionex ICS 1000 system using suppressed conductivity. An anion self-regeneration suppressor (ASRS 300 4 mm) was used with 50 mM KOH as the eluent at 1 mL/min. For analysis of sulfate, the KOH eluent concentration was reduced to 25 mM. The stationary phase was an Ion Pac AS23 Analytical 4 × 250 mm column. An applied current of 200 mA was used with an injection volume of 250 μL and a cell temperature of 35 °C. Six-point target calibration curves were used, and stock target concentrations were measured as a reference for each experiment.

Several types of experiments were used to characterize the binding capacity and affinity of the materials synthesized. Batch experiments were conducted in 20 mL scintillation vials (EPA Level 3; clear borosilicate glass; PTFE/silicone-lined cap). A fixed mass of sorbent was weighed directly into the vial using an analytical balance. Target solutions were added to the sorbents in the vials with a portion of the sample retained for use as a control during HPLC or IC analysis. A series dilution of the retained sample was prepared for generation of a standard curve allowing for analysis of target binding by the sorbents. The vials were incubated on rotisserie mixers. Following incubation, samples were filtered using 25 μm Acrodisc 0.2 μm syringe filters with PTFE membranes. The filtered solutions were analyzed by HPLC or IC, and difference method analysis was applied to determine the target removed from solution.

Columns of the sorbent materials were prepared in BioRad disposable polypropylene columns. Depending on the material under consideration, both gravity flow and controlled flow experiments were conducted. Controlled flow was accomplished using a peristaltic pump. As with batch experiments, HPLC difference analysis was used to determine the target bound. Elution from the columns was accomplished using acetonitrile or methanol for nitroenergetic targets. Commercially available preconcentration sorbents LiChrolute EN (VWR International), Sep-Pak RDX (125–150 μm; Waters Corporation, Milford, MA), and Purolite® A530E and A532E were handled identically to the sorbents prepared in-house. Elution of perchlorate and other ionic targets from the columns was accomplished using aqueous HCl.

RESULTS AND DISCUSSION

The development of sorbent materials is detailed in four major sections. (1) PMO sorbents, the initial focus of the effort, were evaluated based on previous results for nitroenergetic targets. The focus was varying the co-condensed precursor mixture and the imprint template to achieve improved selectivity and binding capacity. (2) Having achieved significant advances in target capture, it was necessary to improve the function of the sorbents in an application format. Hierarchical structures were developed based on optimized PMO approaches to provide essential reductions in backpressure for materials packed as columns. (3) Optimized hierarchical structures were tested at the bench scale in real-world matrices and against environmental samples in order to validate the performance characteristics. (4) Lessons learned

through the development of sorbents for nitroenergetic target capture were applied to development of sorbents for perchlorate. These materials presented distinct challenges for adsorption due to the size and ionic nature of the targets.

PMO Sorbents

The specific morphological characteristics of PMO sorbents can be altered through modification to synthetic parameters such as temperature and acid content. Within a limited range of structural characteristics, however, the most dramatic effects on performance are seen when the pore wall composition is changed. There are two avenues for affecting major changes involving alteration to either the precursor composition or the structure directing template. The impacts of variations along each of these lines are addressed in two sections below. The studies presented here build on previous studies directed at the adsorption of nitroenergetic targets. Co-condensation of two precursors was used to improve mesoporosity and morphological character over that achieved in earlier materials. The precursors were selected based on their favorable interaction with nitroenergetic targets [16,17]. In addition, new imprint templates and approaches for their use were evaluated.

Co-condensation

The morphological characteristics (based on nitrogen adsorption) of previously synthesized 100% DEB materials indicated poor access to the mesopore volume due to pore blockage and tortuosity. Surface areas were low and pore sizes were primarily in the micropore range. Uniform pores and high surface areas are desirable for providing optimal access to the functional surface area and improved imprinting efficiency. For this study, several materials, both imprinted and nonimprinted, were synthesized with varying ratios of BTE to DEB (see Table 2). The incorporation of the large organic bridging group (DEB) tends to disrupt the structure of the resulting materials. This can be seen from the decrease in surface areas, pore diameters, and pore volumes when the DEB precursor concentration was increased from 0 to 100% of the total precursor used (Table 2). At 40% DEB (M-60:40), a transition from mesoporous to microporous morphology was noted.

The binding capacity for each co-condensate variant was evaluated through batch type experiments. Materials were incubated in single analyte solutions overnight with agitation in order to determine the total binding capacity for each analyte (TNT, pNP, pCr; Table 3). As expected, the binding capacity of the co-condensates was strongly dependent on the DEB content; unfortunately, as DEB content increased, binding of nontarget compounds also increased. The binding capacity for pNP and pCr remained low for materials with low percent DEB. High DEB concentrations resulted in significant binding of pCr and pNP, considered interferents for the purposes of this effort. All materials attained equilibrium adsorption in less than 30 min. Materials with uniform mesopores, such as M-70:30, were found to reach equilibrium adsorption in less than 3 min.

Competitive binding from target mixtures can be used to provide an indication of the tendency for target (TNT) binding over that of other compounds of similar structure. Table 3 shows the results of experiments using a three-component solution (solution A). While the binding of TNT by M-100:0 and M-90:10 was not impacted by the presence of pCr and pNP in the sample, the other BTE:DEB materials showed a reduction in TNT bound per surface area when the target was presented in the mixed sample. M-70:30 offered a compromise in that it displayed a marked enhancement in TNT binding over that observed with the BTE-only material, but binding of compounds such as pNP and pCr was not strongly increased.

Table 2 — PMO Sorbent Material Characteristics

Material	% DEB[†]	% mod-Brij[@]	Surface Area (m²/g)	Pore Volume (cm³/g)	Pore Diameter (Å)
M-100:0	0	0	1180	1.07	38
M-100:0 Imp	0	12.5	1157	1.07	39
M-90:10	10	0	1071	0.75	28
M-90:10 Imp	10	12.5	1077	0.78	30
M-75:25	25	0	1056	0.63	22
M-75:25 Imp	25	12.5	1075	0.64	23
M-70:30	30	0	1004	0.56	21
M70:30 Imp	30	12.5	1095	0.60	22
M-60:40	40	0	922	0.52	<20
M-60:40 Imp	40	12.5	957	0.52	<20
M-50:50	50	0	813	0.46	<20
M-50:50 Imp	50	12.5	847	0.44	<20
M-0:100	100	0	356	0.20	<20
M-0:100 Imp	100	12.5	317	0.18	<20
M-70:30 Imp 25	30	25	977	0.59	23
M-70:30 Imp 50	30	50	1028	0.63	26
M-70:30 Imp 100	30	100	707	0.59	31

[†]Indicates the percentage of DEB precursor used during synthesis
[@]Indicates the percentage of DNB-modified Brij®76 used to imprint the material

Table 3 — Binding of Targets from Single- and Three-Component Solutions

Material	TNT*		pNP*		pCr*	
	TNT	A†	pNP	A†	pCr	A†
M-100:0	0.34	0.39	0.04	0.09	0.55	0.39
M-100:0 Imp	0.32	0.41	0.00	0.03	0.60	0.29
M-90:10	1.19	1.23	0.24	0.23	0.40	0.28
M-90:10 Imp	1.03	1.18	0.11	0.00	0.37	0.19
M-70:30	3.01	2.07	0.24	0.22	0.77	0.55
M70:30 Imp	2.97	3.42	0.35	0.10	0.74	0.41
M-60:40	4.98	3.49	0.78	0.73	1.25	0.90
M-60:40 Imp	4.97	2.64	0.75	0.22	1.32	0.57
M-50:50	5.98	4.07	0.60	0.73	1.65	1.14
M-50:50 Imp	5.90	3.66	1.59	0.34	1.69	0.72
M-0:100	16.30	12.09	3.07	0.86	10.71	1.65
M-0:100 Imp	19.36	12.08	3.03	0.98	12.93	1.37
M-70:30 Imp 25	2.13	3.19	0.33	0.22	0.63	0.42
M-70:30 Imp 50	2.79	3.80	0.31	0.13	0.71	0.33
M-70:30 Imp 100	5.17	2.44	0.45	0.23	1.38	0.51

*Amount of analyte bound in $\mu g/m^2$

†Sample A contained 22 μM TNT, pNP, and pCr

Imprinting

The idea of imprinting the organosilicate sorbents evolved as a result of the establishment of procedures for molecular imprinting of polymer materials (MIPs). The use of groups in contact with the pore walls during precursor condensation allows PMO materials to be similarly "imprinted." In our previous work, this was accomplished through incorporation of a molecule with a target-like group into the synthesis of DEB-bridged materials as a small percentage of the total surfactant [16,17]. The expectation was that, upon extraction, some target-complementary sites would remain on the pore surfaces. Decylaminetrinitrobenzene was used as the target analog–bearing molecule (Fig. 2), but only marginal success was achieved when it was used for imprinting in combination with Brij®76 surfactant micelles [17]. It seems likely that the overall hydrophobic nature and the short chain length of this molecule resulted in inefficient association of the trinitrobenzene head group with the hydrophilic alkylene oxide head groups of Brij®76 surfactant. The present work sought to overcome the inefficiency of the process through the use of a surfactant modified with the target analog [15]. The effect of incorporating various amounts of this analog into the surfactant micelles was evaluated in order to optimize the resulting materials.

Imprinting the co-condensates with 12.5% DNB-Brij was not found to significantly alter the material characteristics (Table 2). Effectiveness of imprinting was evaluated by comparing the performance of the imprinted materials to that of the nonimprinted materials. Both single- and multiple-target experiments

were employed (Table 3). Binding of targets from single-analyte solutions was similar for the imprinted and nonimprinted materials when less than 50% DEB bridging group was incorporated. An increase in TNT capacity was noted upon imprinting of M-0:100 (M-0:100 Imp in Table 3). The total pNP and pCr binding from single-analyte solutions was not significantly impacted by imprinting. The effect of imprinting was more clearly observed when mixtures of targets were present. While M-100:0 and M-90:10 showed no difference in adsorption of TNT whether from the mixture (solution A) or the single-analyte solution, M-100:0 Imp, M-90:10 Imp, and M-70:30 Imp showed a slight enhancement (~15%) in TNT absorption from the mixed-target solutions. For all cases, pCr and pNP binding from the mixed sample was reduced by a greater amount, as compared to single-analyte samples, for the imprinted materials. This tended to indicate an enhancement in TNT selectivity upon imprinting. These results also indicated that the effectiveness of imprinting varied with percentage of incorporated DEB.

Imprint Variants

In order to determine the optimal imprint molecule concentration, M-70:30 materials were synthesized with 12.5%, 25%, 50%, and 100% of the Brij®76 surfactant replaced by DNB-Brij. This replacement was not found to strongly impact the surface area or pore volume, with the exception of the 100% substitution (Table 2). The average pore diameter of the materials was found to increase with increasing imprint molecule incorporation from 21 Å (no imprint) to 31 Å (100% modified Brij®76). The changes in pore diameter appeared to be consistent with an alteration in the average length of the surfactant molecule employed.

Single analyte and mixed target solutions were employed as described above to determine binding capacities and to obtain estimates of the selectivity for TNT binding over that of similar molecules. Though a consistently increasing or decreasing trend in TNT capacity was expected for the M-70:30 series of materials, this was not observed (Table 3). In fact, the M-70:30 Imp 25 bound less TNT than the other M-70:30 materials from the single target solution. M-70:30 Imp 100 demonstrated marked improvement in TNT and DNT binding capacity as well as a slight enhancement in RDX binding capacity (Table 4) over the nonimprinted variant. With the exception of the 100% imprint, pNP, pCr, and RDX binding by the materials was minimal compared to TNT binding (Table 3 and Table 4).

The imprint materials were incubated with several mixed sample solutions: TNT, pCr, and pNP (solution A, Table 3); TNT and DNT; TNT and RDX; and DNT and RDX (solutions B, C, and D, Table 4). Evaluation of target binding from solution A indicated that the slight enhancement in TNT binding demonstrated by M-70:30 Imp was consistent for the other imprinted M-70:30 materials with the exception of M-70:30 Imp 100. In the case of the 100% imprint material, a significant decrease in TNT binding was observed when presented as a target mixture (Table 3). Unlike the other sorbents, M-70:30 Imp 100, did not show an XRD reflection, and it produced a broader, less sharply defined nitrogen adsorption pore size distribution compared to the other imprint variants. These morphological differences likely resulted in the unique behavior of M-70:30 Imp 100.

The DNT binding capacity of the M-70:30 materials was found to be comparable to that for TNT (Table 4). DNT was used as an alternative target in these studies because of the structural similarity to the imprint molecule and to TNT. In mixtures of TNT and DNT (solution B, Table 4), DNT was found to compete for TNT binding sites more strongly in the 100% imprint material than in the others, with M-70:30 Imp showing the least impact. Similarly, the presence of TNT had the least impact on DNT binding in M-70:30 Imp. The presence of RDX (solutions C and D) had little effect on either DNT or TNT binding in M-70:30 Imp, while strong competition between all three analytes was noted for the 100% imprint.

Table 4 — Binding of Targets from Single- and Two-Component Solutions

Material	TNT*			DNT*			RDX*		
	TNT	B[†]	C[‡]	DNT	B[†]	D[&]	RDX	C[‡]	D[&]
M-70:30	3.01	2.60	2.95	2.62	2.06	2.79	0.87	0.73	0.47
M70:30 Imp	2.97	2.81	2.61	3.05	3.01	2.95	0.76	0.57	0.76
M-70:30 Imp 25	2.13	1.84	1.97	2.55	2.05	1.99	0.51	0.34	0.04
M-70:30 Imp 50	2.79	2.32	2.54	2.95	2.52	2.77	0.64	0.50	0.43
M-70:30 Imp 100	5.17	4.07	4.38	5.25	4.43	4.85	1.17	0.85	0.91

*Amount of analyte bound in $\mu g/m^2$
[†]Sample B contained 22 μM TNT and DNT
[‡]Sample C contained 22 μM TNT and RDX
[&]Sample D contained 22 μM DNT and RDX

In order to obtain a number indicative of affinity, binding isotherms for the targets were generated based on the Langmuir-Freundlich model (Eq. (1); Fig. 3):

$$q = \frac{q_s k[L]^n}{1 + k[L]^n} \tag{1}$$

From this model, the saturation capacity of the sorbents (q_s), an affinity (k), and an indicator of heterogeneity (n) can be obtained based on the total target bound (q) and the free target concentrations ($[L]$). This model is a generalization of the Langmuir model used to account for surface heterogeneity (nonidentical sites) [33,34]. Good fitting parameters for q_s and k were obtained when the heterogeneity index was fixed at unity (Table 5). Accurate values of n could not be determined due to the limited range of concentrations available from the adsorption experiments.
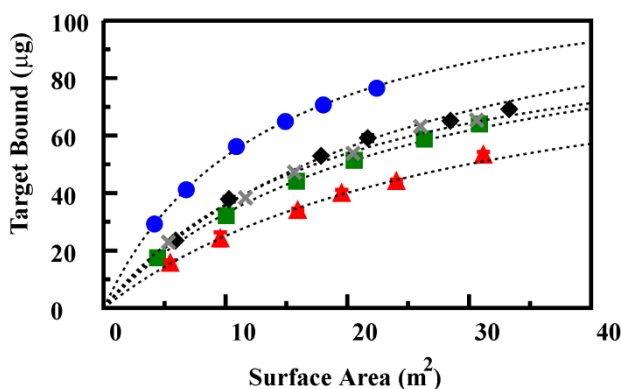

Fig. 3 — Binding isotherms. TNT binding isotherms and the corresponding curve fits are presented for each of the surfactant variants: M-70:30 (×), M-70:30 Imp (♦), M-70:30 Imp 25 (▲), M-70:30 Imp 50 (■), M-70:30 Imp 100 (●). TNT concentration was 22 μM. Curve fit parameters are provided in Table 5.

Table 5 — Langmuir-Freundlich Fit Parameters for TNT Binding Isotherms

Material	q_s (µg/m^2)	k (µg^{-1})
M-70:30	7.66	0.0155
M-70:30 Imp	7.41	0.0179
M-70:30 Imp 25	7.34	0.0076
M-70:30 Imp 50	6.89	0.0154
M-70:30 Imp 100	9.12	0.0396

The method of Ockrent [35] and Weber [36] for prediction of the adsorption of two targets was also applied to determining the heterogeneity of binding sites. In this approach, the following relationship is used:

$$\frac{n_1^{mix}}{n_1^{single}} = 1 - \frac{n_2^{mix}}{n_2^{single}} \qquad (2)$$

where n_1^{mix} is the concentration of target 1 absorbed from the mixture of target 1 and target 2 and n_1^{single} is the concentration of target 1 adsorbed from the single-analyte solution when the total initial target and adsorbent concentrations are fixed at the same value for all solutions. Similarly for n_2, "mix" indicates the two-target solution and "single" indicates the single-analyte solution. Deviation from this relationship indicates heterogeneity; the greater the deviation, the larger the diversity of sites. When this relationship was applied to the data obtained using the imprint variants, M-70:30 Imp 25 was found to display the strongest deviation from the expression Eq. (2). The other four materials performed similarly to one another with deviations of less than 0.15 from the linear function. The calculated association constants from Eq. (1) demonstrate an unexpected trend in the materials (Table 5). While M-70:30 Imp 100 was superior to the other materials in terms of saturation capacity and association constant, the saturation capacity of the other materials decreased with increasing imprint molecule concentration from 0 to 50%. These trends may have resulted from surfactant partitioning during synthesis of the materials.

The binding capacity of the co-condensates depends on the DEB content of the materials; however, as the DEB content of the materials increases, the binding of nontarget compounds also increases. M-70:30 offered a compromise in that it displayed a marked enhancement in TNT binding over that observed with the BTE-only material while binding of compounds such as pNP and pCr was not strongly increased. In addition, imprinting of M-70:30 (M-70:30 Imp; 12.5% DNB-Brij) produced TNT binding which was apparently independent of the presence of pNP and pCr. M-70:30 Imp 100 provided increased absorption of TNT, but binding was highly nonspecific and was subject to reduction when pNP and pCr were present. A sacrifice in total capacity is necessary to obtain the needed selectivity. M-70:30 Imp appears to offer the best combination of TNT binding capacity and selectivity. The new template used for synthesis of these materials greatly improved the impact of the templating process. The technique is also adaptable for generation of templates against other targets of interest, as well as to syntheses that employ other surfactants.

Hierarchical Sorbents

While PMO sorbents provide the desired binding characteristics for TNT, the mesoporous nature of the materials presents disadvantages for their application in in-line preconcentration formats. Small particle sizes result in dense packing. When combined with poor interconnectivity and small pore sizes (~30 Å), flow in a column format experiences high backpressure levels. Mixing with sand or other such materials can resolve this issue, but these approaches also lead to reduced active site concentration within the column. Materials may also slowly compact at the end of the column, resulting in increasing backpressure over time. We applied the lessons learned with the PMO sorbents to the development of a new type of material with a view toward addressing this issue [29]. This material uses a larger surfactant (Pluronic P123) with a swelling agent to effect a process called spinodal decomposition during synthesis. The result is a hierarchical sorbent with mesopores organized within macropores to provide improved access and reduced pressure.

Material Characteristics

Two hierarchical sorbent materials were synthesized and evaluated: MM1 and P10. Fig. 4 presents SEM and TEM images of the MM1 hierarchical material. This material utilizes a 50:50 BTE:DEB ratio with 12.6% imprint template. The SEM image (panel A) clearly shows pores of approximately 1 µm. Bands of lighter and darker regions in the TEM image (panel B) are indicative of ordered pore structure. XRD further confirms the presence of ordered mesopores (panel F). The sharp profile of the primary reflection, as well as the presence of additional reflections in the spectrum, indicate increased mesoscale order over PMO sorbents. This increase in order on the mesoscale typically provides improved access to the pore volume in a material. The increase in order is unexpected considering the concentration of DEB in MM1. For the PMO sorbents, using 50% DEB with 50% BTE resulted in poor material characteristics and a greater degree of disorder (blue line in panels D, E, F). Nitrogen sorption analysis of MM1 yielded a type IV isotherm with uniform pore sizes (panels D, E). The surface area of MM1 (366 m^2/g) is reduced in comparison to the mesoporous material prepared with the same precursor mixture (813 m^2/g) as expected with losses due to the macroscale structure. Mesopore volume is also reduced (from 0.46 cm^3/g to 0.26 cm^3/g for MM1), while the average pore size diameter is increased (from microporous to 35 Å for MM1).

An alternative material, P10, incorporates terminal phenyl groups (PTS) into the hierarchical material. The terminal phenyl groups provide potential binding sites that extend further outside of the electric double layer of the sorbent surface. This material has reasonable materials characteristics, but is missing the macroporous characteristics observed for MM1. An SEM image of P10 is presented in Fig. 4 (panel C). TEM imaging did not reveal ordered pores on the mesoscale. Nitrogen sorption analysis of P10 yielded a type IV/type I isotherm with surface area 276 m^2/g, pore volume 0.226 cm^3/g, and average pore diameter 43 Å (panels D, E). The XRD spectrum for P10 is presented in panel F.
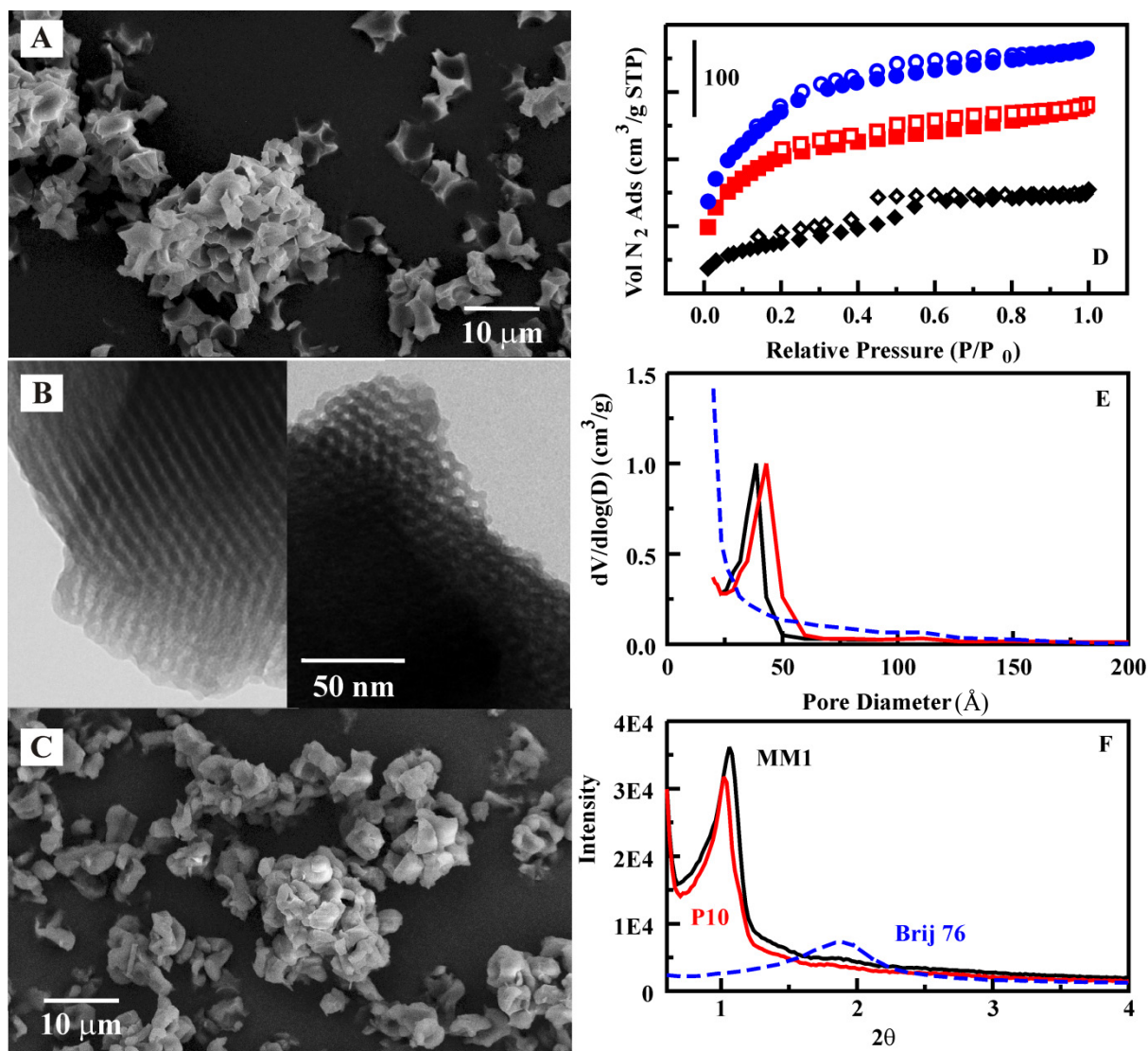
Fig. 4 — Hierarchical material characteristics. Shown here are SEM (panel A) and TEM (panel B) images of MM1 and an SEM image of P10 (panel C). Also presented are the nitrogen sorption isotherms (panel D) for MM1 (black), P10 (red), and the 50:50 BTE:DEB material synthesized using Brij®76 (blue). Open symbols are for desorption, and filled symbols are for sorption. The pore diameter distributions (panel E) and XRD spectra (panel F) are presented as well.

Adsorption Experiments

Binding isotherms for RDX and TNT by P10 and MM1, respectively, are presented in Fig. 5 (panel A). Binding kinetics for these materials (panel B) were slower than those of the PMO sorbents. A period of 20 min was necessary to achieve 95% of maximal target binding. The reasons for the difference in rate are unclear. Analysis of binding site homogeneity was conducted based on the method described above (Eq. (2)). TNT and RDX binding (for MM1 and P10, respectively) in the presence of p-cresol were evaluated (Fig. 6). When the evaluated targets bind to the same sites, this plot is typically linear. When targets are bound by differing sites, there is divergence from the line. On the basis of this data, it appears unlikely that compounds with structures similar to p-cresol will compete with targets (TNT or RDX) for binding sites. This semiselectivity of MM1 was expected based on the results obtained for the PMO sorbents.
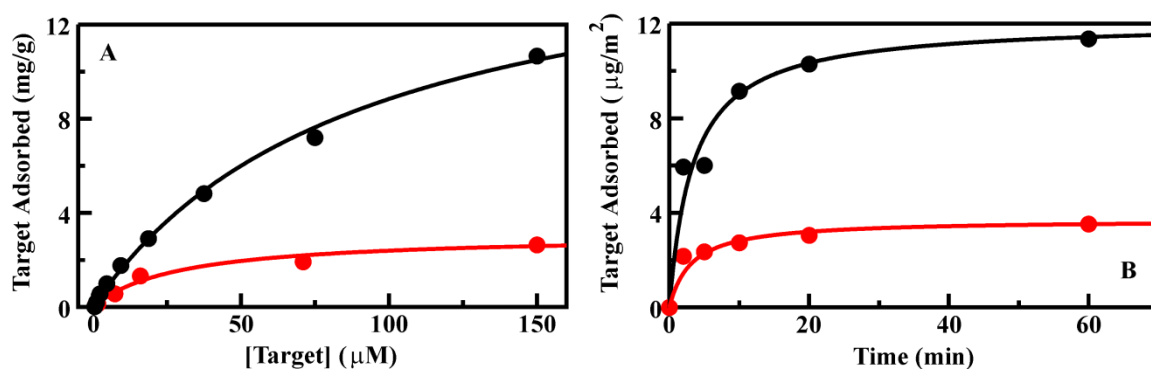

Fig. 5 — Target binding. (Panel A) Standard binding isotherms for TNT by MM1 (black) and RDX by P10 (red). (Panel B) Kinetics for binding of TNT and RDX by MM1 (black) and P10 (red), respectively.
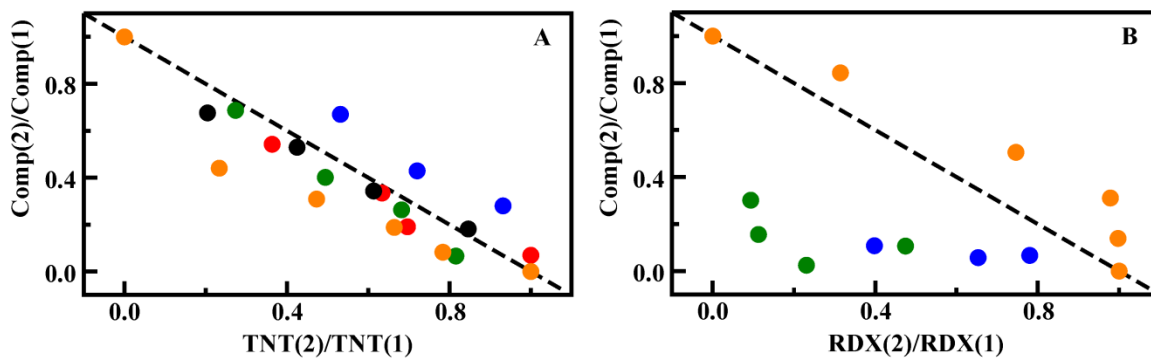

Fig. 6 — Competitive binding. From Eq. (2), these graphs show competitive binding of targets by MM1 in mixtures with TNT (panel A) and P10 in mixtures with RDX (panel B). Here, "comp" indicates the competitive target: pCr (blue), NG (red), pNP (green), DNT (black). Orange points indicate competition between TNT and RDX.

TNT, DNT, RDX, and nitroglycerin are commonly found as co-contaminants. Additional competitive binding experiments were performed using mixtures of these targets (Fig. 6). The concentrations used for these experiments are well below the binding capacity of the material for all of the evaluated targets. Results indicate that TNT and RDX are bound by differing sites within the materials. TNT, DNT, p-nitrophenol, and nitroglycerin, on the other hand, all interact with the same sites. Competition between TNT and DNT is expected due to their very similar structures. RDX is much more rigid than the nitroglycerin structure, which may result in reduced affinity for the compound at the sites of high affinity for TNT. These results are valid under the conditions evaluated; however, competition for sites of lower TNT affinity would be likely at higher target loading levels.

Numbers indicative of affinity for these materials were generated based on fitting by the Langmuir-Freundlich model isotherm (Eq. (1)). In the case of MM1, the heterogeneity index was 0.83 (unlike the PMO sorbents, for which a value of 1 was obtained). This tends to indicate that TNT is bound by sites of varying affinity. In the case of RDX binding by P10, a heterogeneity coefficient of 0.87 yields a good fit. The TNT saturation capacity of MM1 was significantly higher than that of the PMO sorbents (70 $\mu g/m^2$ compared to 3.3 $\mu g/m^2$). RDX capacity was much lower, likely due to the lack of interaction with the π-bonds of the DEB bridging group. Further evidence of these differences was provided by the competitive binding data (above and Fig. 6) and the difference in binding affinity (MM1, 0.003 μg^{-1}; P10, 0.046 μg^{-1}).

Batch experiments were performed in artificial sea water and in pond water collected locally (Alexandria, Virginia) to obtain an idea of the potential for application of these materials to targets in complex matrices. Water samples were spiked with TNT or RDX. While the binding of TNT by MM1 was slightly reduced by the pond water matrix, the binding of RDX by P10 was completely abrogated in both of the matrices. As a result, P10 will not be useful for application outside of a laboratory situation. MM1 is expected to perform under a range of different sample conditions. Binding of TNT by MM1 was not impacted by varying pH (Fig. 7). Increasing temperature, however, reduced the amount of target bound. This is likely due to the decreased residence time of the target on the sorbent surface.
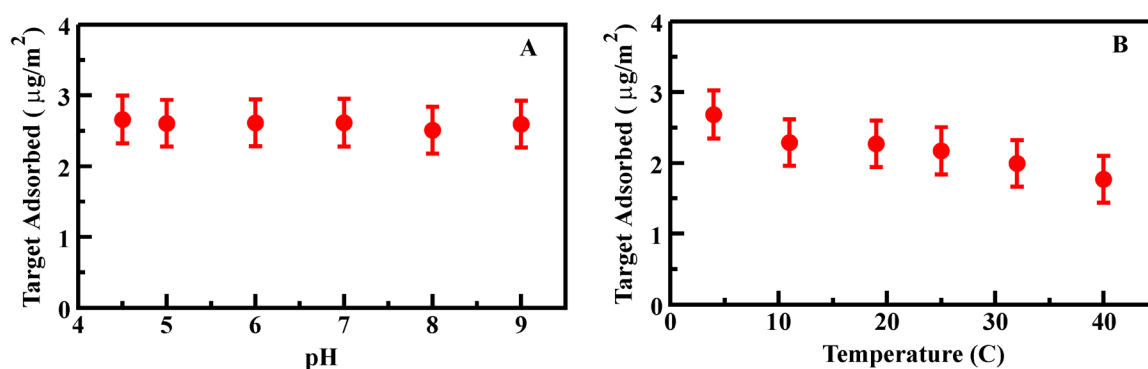

Fig. 7 — Effects of pH and temperature on target binding. (Panel A) Altering the pH of samples through addition of phosphate buffer had little impact on the binding of TNT by MM1. (Panel B) As sample temperature increased, TNT binding by MM1 decreased.

Column Adsorption

Hierarchical sorbents were packed as 200 mg columns to evaluate their potential for application to preconcentration. Columns were characterized by measuring breakthrough capacity and elution characteristics in comparison to activated charcoal (Fig. 8). MM1 and P10 performed similarly in the column format. The total TNT binding capacities for the 200 mg columns were found to be approximately 530 μg (2.6 mg/g). The total RDX binding capacity was found to much less (46 μg for MM1 and 67 μg for P10). Initial TNT breakthrough for P10 was noted at 400 μg and for MM1 at 450 μg. Initial RDX breakthrough for P10 was noted at 25 μg and for MM1 at 50 μg. Partial breakthrough for both targets was noted from the first application on the activated charcoal column, but total capacity was not reached for the carbon for either target (>700 μg). Based on the calculations described above, TNT breakthrough on MM1 was expected at 5 mg; MM1 bound significantly less TNT than expected under the conditions used for the column experiments.

MM1 was also compared to two commercially available preconcentration sorbents, LiChrolut EN and Sep-Pak. Samples of TNT solution in deionized water were applied to 200 mg columns of each of the sorbents. No breakthrough was observed for any of the materials. Elution was accomplished using 1 mL of acetonitrile (based on directions provided for LiChrolut and Sep-Pak). The concentration of TNT recovered upon elution from MM1 was greater than that obtained from either of the commercial sorbents for all applied volumes. Elution of targets from MM1 was also possible using methanol with similar recovery. The recovery of TNT using MM1 for greater than 120 capture/elution cycles showed no degradation in performance for the sorbent.
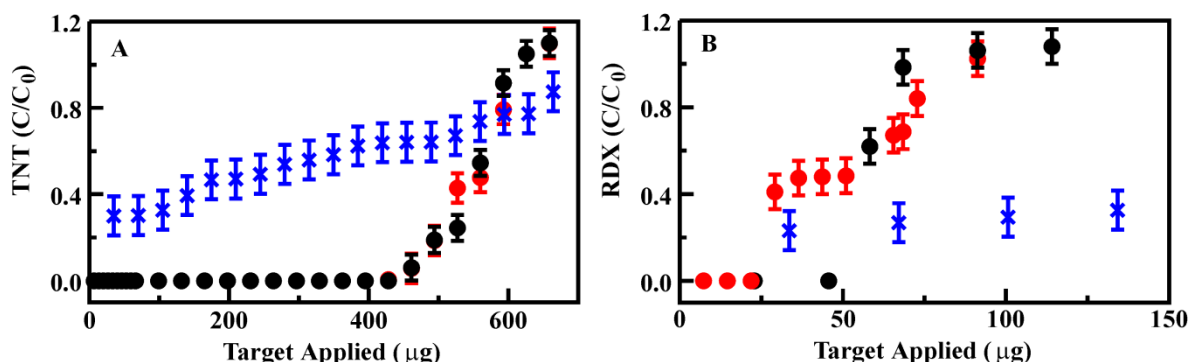

Fig. 8 — Column breakthrough. (Panel A) TNT breakthrough for MM1 (black), P10 (red), and activated charcoal (blue). (Panel B) RDX breakthrough for the same sorbents.

Environmental Samples

Having made significant improvements in the sorbent characteristics and demonstrated their performance in laboratory samples, it was of interest to evaluate performance in real-world matrices [31]. These evaluations were completed in parallel with evaluation of LiChrolut EN and Sep-Pak RDX as representatives of state-of-the-art preconcentration materials. Because nitroenergetic targets in general are of interest for this application, the target list was expanded to include TNT, RDX, HMX, DNT, and NG. These targets have relevance for water quality at munitions testing and training sites as well as sites of storage and manufacture. A baseline for performance was established using samples spiked into deionized

water. HPLC analysis was utilized, and spiked target concentrations were selected to cover those within and below the range of the analytical method (0.9 to 200 ppb). In all cases, 20 mL of the target solution was applied to the column, it was rinsed with deionized water (6 mL), and target was eluted in 4 mL acetonitrile. The column was rinsed with acetonitrile (4 mL) and water (6 mL) prior to application of the next sample. All of the volumes (effluent, eluent, and rinses) were analyzed by HPLC. Fig. 9 (panel A) provides a comparison of the performance of MM1 to the commercial sorbents. Overall, MM1 (blue) provided effective capture and elution of TNT, RDX, DNT, and NG. Results were comparable to the LiChrolut sorbent (red) and exceeded those of the Sep-Pak sorbent (black). None of the materials performed well for HMX. Table A1 provides detailed results for all spiked deionized water samples. Commercial sorbents performed poorly against NG. Sep-Pak showed target breakthrough and bleeding into washes for nearly all compounds.
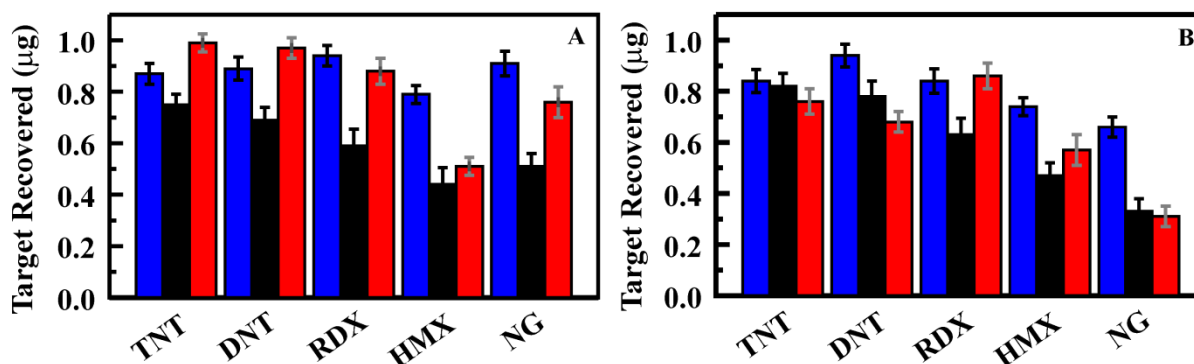

Fig. 9 — Target preconcentration. (Panel A) Target recovered in the eluent for each of the three sorbents from targets in deionized water. (Panel B) Target recovered in the eluent for each of the three sorbents from targets in artificial sea water. MM1 (blue), Sep-Pak (black), LiChrolut (red). Applied target at 50 ppb.

Samples prepared in artificial sea water and in natural water samples (ground and surface) were also evaluated. Fig. 9 (panel B) presents representative results for samples in artificial sea water; Table A2, Table A3, and Table A4 provide results for samples in sea water, groundwater, and surface water, respectively. For MM1, recovery of targets from artificial sea water was similar to that observed for deionized water samples, indicating that target binding is not dependent on ionic strength. Recovery of TNT and DNT by LiChrolut was reduced in this matrix while recovery of RDX and HMX was not. Recovery of RDX, HMX, TNT, and DNT by Sep-Pak was slightly increased in artificial sea water. NG recovery was negatively impacted for all sorbents. Surface water (pond; Table A4) and groundwater (well; Table A3) samples were filtered prior to spiking. For MM1, recovery of DNT, TNT, and RDX from these matrices was similar to that from deionized water. HMX and NG recovery were reduced. TNT, DNT, and NG recovery by LiChrolut was negatively impacted with little change in RDX and HMX recovery. Sep-Pak performance was poor for both matrices. Because of the potential for varied pH in water samples, recovery of targets at pH 3.0 and 9.0 was also evaluated (Table A5). For MM1, recovery of TNT, HMX, and NG were reduced at low pH, with only slight effects observed at high pH. Low pH had a stronger impact on LiChrolut performance and little impact on Sep-Pak performance.

Soil samples were provided by A.D. Hewitt from former munitions testing sites on Holloman Air Force Base (Table A6). Samples contained various contaminants at differing concentrations. Sample sites varied in the size of ordnance and the age of the site. The samples were handled and analyzed in

accordance with EPA Method 8330B by the Engineer Research and Development Center, U.S. Army Corps of Engineers. Complete results of this analysis are provided in Table A7. The soils were extracted into water to prepare samples for analysis. If sample HO-004 is taken as an example, the EPA method indicated a high concentration of TNT and lower concentrations of RDX and DNT as well as trace amounts of 2-amin-4,6-dinitrotoluene (2-ADNT) and 4-amino-2,6-dinitrotoluene (4-ADNT). When preconcentration of this sample was attempted with the MM1 sorbent column, TNT in the sample saturated the sorbent, resulting in some TNT found in the column effluent. The concentration in the eluent was enhanced by nearly ten times (Table A8). Trinitrobenzene (TNB), 2-ADNT, and 4-ADNT were below the detectable limit in the as-extracted sample, but were detected in the eluent following preconcentration. The concentration of RDX was enhanced by seven times. Target concentration enhancements by MM1 were impacted by the affinity of the sorbent for the targets and by the relative concentrations in the mixed samples. Comparative data for the commercial sorbents on a single soil extract is provided in Table A9.

Sorbents for Perchlorate

Binding of nitroenergetic targets by the NRL-developed sorbents is accomplished through hydrophobic/hydrophilic interactions, π–π stacking, and other target surface interactions. Capture of perchlorates requires interaction via a charged group. Commercial materials are typically strong base resins that provide no selectivity. Other materials using alkylammonium groups have been described with similar results [18,32]. The goal of the present work was to combine the characteristics of the hierarchical materials with ion exchange sites in order to provide selectivity in perchlorate capture. N-trimethoxysilylpropyl-N, N, N-trimethylammonium chloride (M) and N-trimethoxysilylpropyl-N, N, N-tri-n-butylammonium (B) were grafted onto silicate scaffolds of varying morphological characteristics. Like the materials described above, these materials are hierarchical. The HX material offers hexagonally packed cylindrical pores while CF is a mesostructured cellular foam, a more disorganized structure. Fig. 10 provides characterization data for the materials. Average pore sizes of 77 Å and 111 Å were obtained for HX and CF, respectively. Grafting of the reactive groups had significant impact on pore size, pore volume, and surface area (Table A10). A complex dependence was noted between binding capacity and site loading. Site loading at high levels likely results in restricted access to portions of the pore volume. Loading on the HX and CF materials also produced significantly different results. On a per gram basis, HX had a significantly higher binding capacity than the CF sorbent. On a per surface area basis, the CF materials appeared to be the stronger performers. This may be due to varying restrictions and steric hindrance in regions of the HX sorbents.

Redesign of the sorbent scaffold through variation of the mesitylene concentration used during synthesis yielded two additional materials, CF2 and CF3, with differing morphologies and pore sizes (Table A10). Several variants of the HX and CF materials were produced, listed in Table A10; the nomenclature reflects the base material followed by the mmol quantity of alkylammonium group (B or M) used in the grafting step. The CF3-4M variant bound 13% more perchlorate than the CF4M variant (Table A11) with only a marginal increase in surface area. Batch experiments were conducted using several of the prepared variants to evaluate binding of perchlorate, nitrate, perrhenate, thiocyanate, sulfate, and phosphate (Table A11). Binding ratios for the targets varied widely between the different materials. Commercial sorbents Purolite A530E and A532E, the strong base resins, were also evaluated. The binding capacity of the commercial sorbents was significantly greater than that of the CF and HX sorbents.

Binding isotherms were generated for the HX and CF materials based on Eq. (3) [37]:

$$[Perchlorate]_{Bound} = \frac{\frac{K_P}{1+K_C[Chloride]_{Free}}[Sites]_{Total}[Perchlorate]_{Free}}{1+\frac{K_P}{1+K_C[Chloride]_{Free}}[Perchlorate]_{Free}} \qquad (3)$$

where K_P and K_C are the site affinity for perchlorate and chloride, respectively. Here, site concentration was a variable to be determined with the volume and mass of sorbent as known quantities. This allowed for calculation of the sites (mole) per gram of sorbent. An example of experimental and calculated data is presented in Fig. 11. Table A12 provides the calculated constants for each of the materials. From Table A12, it is clear that a given type of functional group (B or M) leads to differing affinity in the different materials. It is also necessary to note that functionalization with a higher concentration of a ligand does not necessarily result in higher site loading; for example, HX2M has 1.86 mmol/g and HX4M has 0.45 mmol/g. The blockage of pores by higher loading is supported by a loss in surface area (321 m^2/g versus 232 m^2/g).

The relationship in Eq. (2) can be applied to binding of ionic targets from mixed solutions to determine if various targets bind similar sites within the materials. Fig. 11 provides an example of this type of data. Results indicated that CF3-4M, CF2-4M, and HX2M preferentially bound perchlorate over perrhenate or thiocyanate. CF4M, CF1M3B, and HX1M3B preferentially bound perrhenate over perchlorate but bound similar amounts of perchlorate and thiocyanate. This result again illuminates the variability in binding related to the environment of the binding site within the sorbents (curvature, crowding, etc.). Because CF4M, CF2-4M, and CF3-4M showed the greatest degree of preferential binding, they were evaluated in column format (Fig. 11, panels C, D). Overall, CF3-4M offered greater capacity than the other sorbents and a delayed breakthrough profile. When combined with the selective binding characteristics, CF3-4M offers a desirable combination of characteristics. Perchlorate breakthrough was also evaluated for the commercial resins. Though the capacity of those materials was significantly higher than CF3-4M, breakthrough was noted from the initial application.

A CF3-4M column was used for preconcentration of perchlorate single-target and two-target solutions. Targets were applied as 50 mL samples and elution was accomplished using 2 mL 0.2 M HCl. The resulting data set is provided in Table A13. Complete capture and elution would result in a concentration enhancement of 25 times; here, an enhancement of 14 times (on average) was achieved with linear dependence on applied concentration. Increased HCl concentration in the eluent may improve this result. The IC method applied here could not be utilized with greater HCl concentrations. A series of samples containing mixtures of perchlorate and perrhenate or thiocyanate at varying concentrations was also evaluated (Table A14). The recovery of perchlorate in the presence of perrhenate was not statistically different from perchlorate recovery from single-target solutions. The presence of thiocyanate, however, did significantly reduce the recovery of perchlorate.

Binding of perchlorate and other ionic targets was found to vary significantly between silicate sorbents functionalized with combinations of two alkylammonium groups. Differences were observed even for sorbents functionalized at similar loading levels of identical groups. From these results, it seems that factors such as surface curvature and site crowding influence the performance of the sorbents. Through combinations of these effects it was possible to generate a sorbent with affinity for perchlorate that was higher than that for other ionic targets such as perrhenate. The selected sorbent was applied in a column format to extraction of perchlorate from spiked solutions including those with two targets and those prepared using groundwater. While perchlorate binding capacity in the sorbents developed here was less than that of the commercial resins, these sorbents offer several advantages. First, the silicate sorbents

favor perchlorate binding over perrhenate; Purolite resins favor perrhenate. Second, the silicate sorbents more effectively capture perchlorate at low concentrations, simplifying quantitative analysis of concentrations. Finally, elution of perchlorate from the silicate sorbents can be achieved using only hydrochloric acid. This eliminates the need for the post-processing steps necessary for iron-containing eluents utilized with commercial resins.
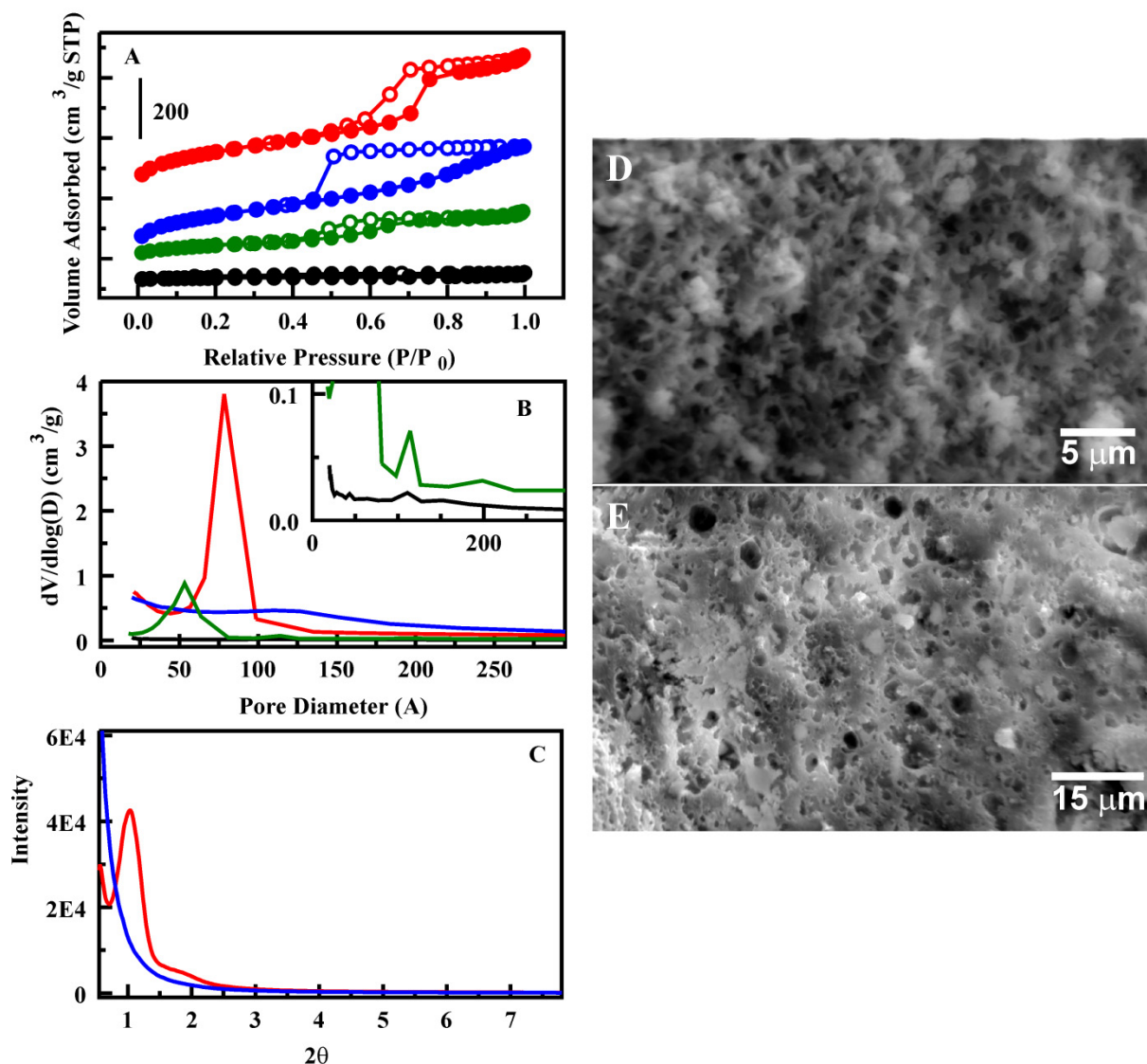

Fig. 10 – Materials characterization for perchlorate sorbents. (Panel A) Nitrogen sorption isotherms for HX (red, shifted +200), CF (blue, shifted +110), HX1M3B (green), and CF1M3B (black) sorbents. (Panel B) Pore size distributions for HX (red), CF (blue), HX1M3B (green), and CF1M3B (black). The inset shows a zoom view of the HX1M3B and CF1M3B pore size distributions. (Panel C) X-ray diffraction patterns for HX (red) and CF (blue) sorbents. SEM images of HX (panel D) and CF (panel E) show differing macroscale morphologies.
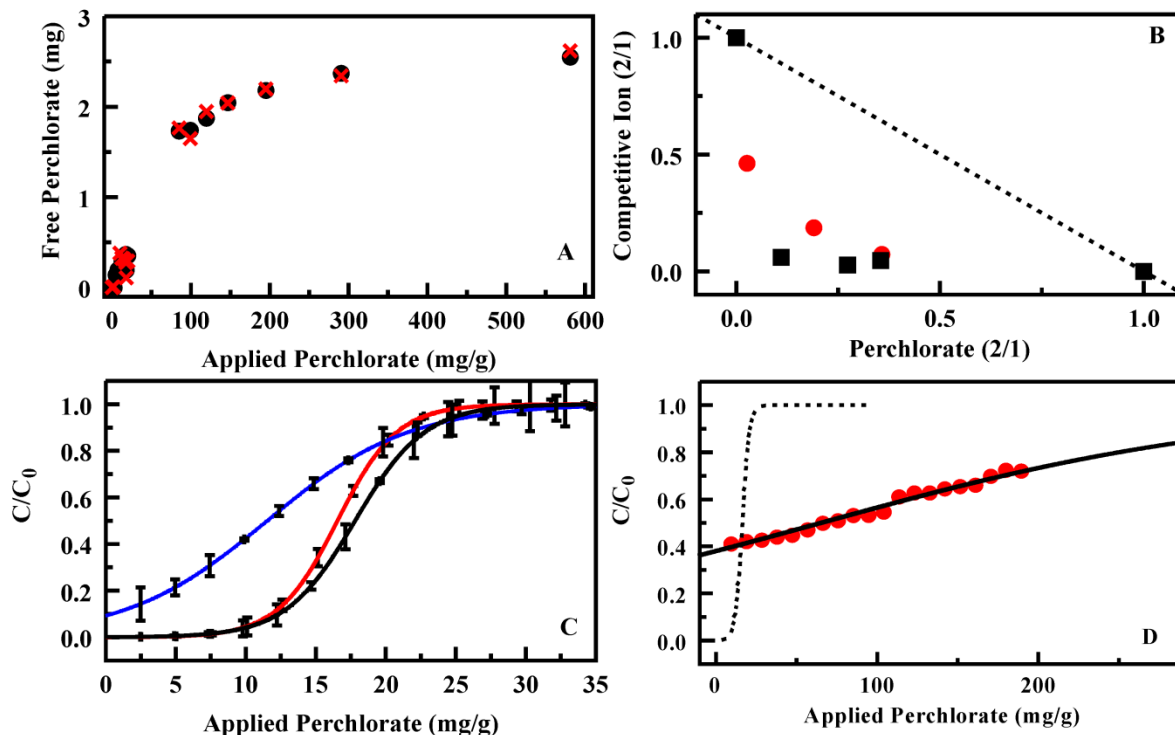
Fig. 11 – (Panel A) Perchlorate binding by CF4M from batch experiments. Shown are experimental data (black) and the results of fitting that data (red). (Panel B) Competitive ion binding from mixed target solutions by CF3-4M: binding from solutions of perchlorate and perrhenate (red) and binding from solutions of perchlorate and thiocyanate (black). (Panel C) Perchlorate breakthrough for 200 mg columns of CF4M (red), CF2-4M (blue), and CF3-4M (black). (Panel D) Perchlorate breakthrough for 50 mg column of Purolite A530E (dashed line is CF4M data).

CONCLUSIONS

The sorbents developed for application to nitroenergetic targets show strong performance, with improvements over the commercially available materials. MM1 showed less sensitivity to matrix conditions than the commercial resins, with 14% to 24% greater target recovery than the other resins evaluated. Preconcentration of targets by one order of magnitude was demonstrated. Further concentration enhancement is possible when larger sampling volumes are utilized. MM1 represents a number of advancements in sorbent development including improved imprinting, enhanced structure through co-condensation, and hierarchical morphology. These features combine to provide a sorbent that is rugged and stabile, highly reusable, and specifically applicable to the preconcentration of nitroenergetic targets. The next step in the development of these materials is to generate the systems and protocols necessary for their application with portable, in-line sensing.

The perchlorate directed materials combine standard approaches and utilize morphological features such as surface curvature to influence the performance of standard binding moieties. Though the sorbents have a lower total binding capacity than the commercial resins, they offer improved target retention at low concentrations and selectivity for perchlorate over other ionic targets. Elution from the sorbents can be accomplished with hydrochloric acid rather than with the iron-containing eluents necessary with the commercial resins, a critical aspect for forensics type applications. These features combine to offer significant advantages to perchlorate analysis and source identification. While electrochemical analysis is

not applicable to this target, preconcentration using the sorbents could be used in-line with ion selective electrodes to achieve portable sensing.

ACKNOWLEDGMENTS

REFERENCES

1. "Nitroaromatics, Nitramines, and Nitrate Esters by High Performance Liquid Chromatography (HPLC)," Method 8330B, U.S. Environmental Protection Agency, Washington, DC, 2006.

2. K. Nagatomo, T. Kawaguchi, N. Miura, K. Toko, and K. Matsumoto, "Development of a sensitive surface plasmon resonance immunosensor for detection of 2,4-dinitrotoluene with a novel oligo (ethylene glycol)-based sensor surface," *Talanta* **79**, 1142–1148 (2009).

3. G.P. Anderson and E.R. Goldman, "TNT detection using llama antibodies and a two-step competitive fluid array immunoassay," *J. Immunol. Methods* **339**, 47–54 (2008).

4. J. Wang, "Electrochemical sensing of explosives," *Electroanal.* **19**, 415–423 (2007).

5. E.J. Poziomek, J. Homstead, and S.H. Almeer, "Quality issues in the use of ion mobility spectrometry," *Proc. SPIE* **3575**, 403–413 (1998).

6. J. Wang, R.K. Bhada, J.M. Lu, and D. MacDonald, "Remote electrochemical sensor for monitoring TNT in natural waters," *Analytica Chimica Acta* **361**, 85–91 (1998).

7. S. Armenta, M. Alcala, and M. Blanco, "A review of recent, unconventional applications of ion mobility spectrometry (IMS)," *Analytica Chimica Acta* **703**, 114–123 (2011).

8. J.M. Perr, K.G. Furton, and J.R. Almirall, "Solid phase microextraction ion mobility spectrometer interface for explosive and taggant detection," *J. Sep. Sci.* **28**, 177–183 (2005).

9. K. Cottingham, "Ion mobility spectrometry rediscovered," *Anal. Chem.* **75**, 435A–439A (2003).

10. A.B. Kanu, H.H. Hill, M.M. Gribb, and R.N. Walters, "A small subsurface ion mobility spectrometer sensor for detecting environmental soil-gas contaminants," *J. Environ. Monitor.* **9**, 51–60 (2007).

11. "Explosives in Water Field Screening Technologies UMDA and SUBASE Bangor," U.S. Environmental Protection Agency, Black and Veatch Special Projects Corp., Tacoma, WA, 1996.

12. T.F. Jenkins, P.G. Thorne, and M.E. Walsh, "Field Screening Method for TNT and RDX in Groundwater," U.S. Army Corps of Engineers, Hanover, NH, 1994.

13. R.J.P. Corriu and D. Leclercq, "Recent developments of molecular chemistry for sol-gel processes," *Angewandte Chemie International Edition* **35**, 1420–1436 (1996).

14. Q.S. Huo, D.I. Margolese, and G.D. Stucky, "Surfactant control of phases in the synthesis of mesoporous silica-based materials," *Chem. Mater.* **8**, 1147–1160 (1996).

15. B.J. Johnson, B.J. Melde, P.T. Charles, D.C. Cardona, M.A. Dinderman, A.P. Malanoski, and S.B. Qadri, "Imprinted nanoporous organosilicas for selective adsorption of nitroenergetic targets," *Langmuir* **24**, 9024–9029 (2008).

16. B. Johnson-White, M. Zeinali, A.P. Malanoski, and M. Dinderman, "Sunlight catalyzed conversion of cyclic organics with novel mesoporous organosilicas," *Catal. Commun.* **8**, 1052–1056 (2007).

17. B. Johnson-White, M. Zeinali, K.M. Shaffer, J.C.H. Patterson, P.T. Charles, and M.A. Markowitz, "Detection of organics using porphyrin embedded nanoporous organosilicas," *Biosens. Bioelectron.* **22**, 1154–1162 (2007).

18. K. Nakanishi, T. Amatani, S. Yano, and T. Kodaria, "Multiscale templating of siloxane gels via polymerization-induced phase separation," *Chem. Mater.* **20**, 1108–1115 (2008).

19. B.J. Johnson, B.J. Melde, C. Thomas, A.P. Malanoski, I.A. Leska, P.T. Charles, D.A. Parrish, and J.R. Deschamps, "Fluorescent silicate materials for the detection of paraoxon," *Sensors* **10**, 2315–2331 (2010).

20. B.J. Johnson, N.E. Anderson, P.T. Charles, A.P. Malanoski, B.J. Melde, M. Nasir, and J.R. Deschamps, "Porphyrin-embedded silicate materials for detection of hydrocarbon solvents," *Sensors* **11**, 886–904 (2011).

21. B. Johnson-White, L. Buquo, M. Zeinali, and F.S. Ligler, "Prevention of nonspecific bacterial cell adhesion in immunoassays by use of cranberry juice," *Anal. Chem.* **78**, 853–857 (2006).

22. M.C. Burleigh, M.A. Markowitz, M.S. Spector, and B.P. Gaber, "Porous polysilisesquioxanes for the adsorption of phenols," *Environ. Sci. Technol.* **36**, 2515–2518 (2002).

23. M.C. Burleigh, S. Jayasundera, C.W. Thomas, M.S. Spector, M.A. Markowitz, and B.P. Gaber, "A versatile synthetic approach to periodic mesoporous organosilicas," *Colloid Polym. Sci.* **282**, 728–733 (2004).

24. A. Nozawa and T. Ohnuma, "Improved high-performance liquid-chromatographic analysis of ethylene-oxide condensates by their esterification with 3,5-dinitrobenzoyl chloride," *J. Chromatogr.* **187**, 261–263 (1980).

25. C. Sun, M. Baird, H.A. Anderson, and D.L. Brydon, "Separation and determination of oligomers and homologues of aliphatic alcohol ethoxylates in textile lubricants and lubricant emulsion by high-performance liquid chromatography," *J. Chromatogr. A* **771**, 145–154 (1997).

26. C. Sun, M. Baird, and J. Simpson, "Determination of poly(ethylene glycol)s by both normal-phase and reversed-phase modes of high-performance liquid chromatography," *J. Chromatogr. A* **800**, 231–238 (1998).

27. B.J. Johnson, I.A. Leska, B.J. Melde, and J.R. Taft, "Removal of phosgene by metalloporphyrin-functionalized porous organosilicates " *Catal. Commun.* **27**, 105–108 (2012).

28. K. Nakanishi, Y. Kobayashi, T. Amatani, K. Hirao, and T. Kodaira, "Spontaneous formation of hierarchical macro-mesoporous ethane-silica monolith," *Chem. Mater.* **16**, 3652–3658 (2004).

29. B.J. Johnson, B.J. Melde, P.T. Charles, M.A. Dinderman, A.P. Malanoski, I.A. Leska, and S.A. Qadri, "Macroporous silica for concentration of nitroenergetic targets," *Talanta* **81**, 1454–1460 (2010).

30. B.J. Melde, B.J. Johnson, M.A. Dinderman, and J.R. Deschamps, "Macroporous periodic mesoporous organosilicas with diethylbenzene bridging groups," *Micropor. Mesopor. Mat.* **130**, 180–188 (2010).

31. B.J. Johnson, B.J. Melde, I.A. Leska, P.T. Charles, and A.D. Hewitt, "Solid-phase extraction using hierarchical organosilicates for enhanced detection of nitroenergetic targets," *J. Environ. Monitor.* **13**, 1404–1409 (2011).

32. T. Amatani, K. Nakanishi, K. Hirao, and T. Kodaira, "Monolithic periodic mesoporous silica with well-defined macropores," *Chem. Mater.* **17**, 2114–2119 (2005).

33. H.J. Kim and G. Guiochon, "Comparison of the thermodynamic properties of particulate and monolithic columns of molecularly imprinted copolymers," *Anal. Chem.* **77**, 93–102 (2005).

34. R.J. Umpleby, S.C. Baxter, M. Bode, J.K. Berch, R.N. Shah, and K.D. Shimizu, "Application of the Freundlich adsorption isotherm in the characterization of molecularly imprinted polymers," *Analytica Chimica Acta* **435**, 35–42 (2001).

35. C. Ockrent, "Selective adsorption by activated charcoal from solutions containing two organic acids," *Journal of the Chemical Society,* 613–630 (1932).

36. W.J. Weber, "Competitive interactions in adsorption from dilute aqueous bi-solute solutions," *Journal of Applied Chemistry of the USSR* **14**, 565–572 (1964).

37. D.J. Winzor, "Determination of binding constants by affinity chromatography," *J. Chromatogr. A* **1037**, 351–367 (2004).

Appendix

DATA TABLES

Table A1 — Recovery of Targets from Deionized Water

Target	[Applied] (ppb)		MM1	Sep-Pak	LiChrolute EN
TNT	200	Eluant	85	71	85
		Total	87	99	98
	50	Eluant	88	75	99
		Total	88	86	99
	5	Eluant	97	88	101
		Total	97	88	101
	0.9	Eluant	ND	ND	ND
		Total	ND	ND	ND
RDX	200	Eluant	92	59	99
		Total	92	96	100
	50	Eluant	94	59	88
		Total	94	128	88
	5	Eluant	96	ND	ND
		Total	96	ND	ND
	0.9	Eluant	ND	ND	ND
		Total	ND	ND	ND
HMX	200	Eluant	78	52	53
		Total	78	81	64
	50	Eluant	79	44	51
		Total	79	89	65
	5	Eluant	ND	ND	56
		Total	ND	ND	56
	0.9	Eluant	ND	ND	ND
		Total	ND	ND	ND
DNT	200	Eluant	91	73	95
		Total	91	107	107
	50	Eluant	89	69	97
		Total	89	92	110
	5	Eluant	90	65	87
		Total	90	65	87
	0.9	Eluant	ND	ND	ND
		Total	ND	ND	ND
NG	200	Eluant	87	57	74
		Total	87	69	74
	50	Eluant	91	51	76
		Total	91	51	76
	5	Eluant	ND	ND	ND
		Total	ND	ND	ND
	0.9	Eluant	ND	ND	ND
		Total	ND	ND	ND

Values provided in percent recovered. ND indicates not detected.

Table A2 — Recovery of Targets from Artificial Sea Water

Target	[Applied] (ppb)		MM1	Sep-Pak	LiChrolute EN
TNT	200	Eluant	90	81	78
		Total	90	93	78
	50	Eluant	84	82	76
		Total	82	82	76
	5	Eluant	72	68	93
		Total	72	68	93
	0.9	Eluant	ND	ND	ND
		Total	ND	ND	ND
RDX	200	Eluant	82	73	86
		Total	93	81	95
	50	Eluant	84	63	86
		Total	84	74	86
	5	Eluant	ND	ND	ND
		Total	ND	ND	ND
	0.9	Eluant	ND	ND	ND
		Total	ND	ND	ND
HMX	200	Eluant	78	51	56
		Total	92	51	61
	50	Eluant	74	47	57
		Total	74	47	56
	5	Eluant	67	ND	52
		Total	67	ND	58
	0.9	Eluant	ND	ND	ND
		Total	ND	ND	ND
DNT	200	Eluant	94	79	81
		Total	94	113	91
	50	Eluant	94	78	68
		Total	94	130	68
	5	Eluant	81	ND	ND
		Total	81	ND	ND
	0.9	Eluant	ND	ND	ND
		Total	ND	ND	ND
NG	200	Eluant	63	41	37
		Total	72	41	37
	50	Eluant	66	33	31
		Total	66	33	31
	5	Eluant	ND	ND	ND
		Total	ND	ND	ND
	0.9	Eluant	ND	ND	ND
		Total	ND	ND	ND

Values provided in percent recovered. ND indicates not detected.

Table A3 — Recovery of Targets from Groundwater

Target	[Applied] (ppb)		MM1	Sep-Pak	LiChrolute EN
TNT	200	Eluant	87	48	57
		Total	87	71	59
	50	Eluant	92	46	60
		Total	92	83	60
RDX	200	Eluant	92	64	81
		Total	92	75	84
	50	Eluant	90	50	71
		Total	90	50	75
DNT	200	Eluant	91	59	71
		Total	91	84	77
	50	Eluant	88	63	73
		Total	88	73	80
HMX	200	Eluant	3	51	41
		Total	70	75	50
	50	Eluant	ND	37	44
		Total	ND	44	54
NG	200	Eluant	86	41	51
		Total	86	41	51
	50	Eluant	74	50	59
		Total	74	50	59

Values provided in percent recovered. ND indicates not detected.

Table A4 — Recovery of Targets from Surface Water

Target	[Applied] (ppb)		MM1	Sep-Pak	LiChrolute EN
TNT	200	Eluant	89	46	52
		Total	89	66	55
	50	Eluant	87	63	83
		Total	87	85	91
RDX	200	Eluant	89	82	82
		Total	90	66	87
	50	Eluant	84	63	90
		Total	84	70	90
DNT	200	Eluant	89	72	87
		Total	90	111	92
	50	Eluant	87	71	89
		Total	87	84	98
HMX	200	Eluant	55	49	61
		Total	55	82	73
	50	Eluant	50	30	51
		Total	50	30	73
NG	200	Eluant	81	59	60
		Total	81	59	60
	50	Eluant	85	53	54
		Total	85	53	54

Values provided in percent recovered.

Table A5 — Recovery of Targets from Samples of Varied pH

Target	pH	[Applied] (ppb)		MM1	Sep-Pak	LiChrolute EN
TNT	3	200	Eluant	77	44	60
			Total	77	78	67
		50	Eluant	70	51	56
			Total	70	65	67
	9	200	Eluant	84	73	68
			Total	97	86	76
		50	Eluant	85	59	62
			Total	85	72	74
RDX	3	200	Eluant	86	58	74
			Total	86	76	78
		50	Eluant	86	55	63
			Total	86	63	66
	9	200	Eluant	97	64	80
			Total	97	71	82
		50	Eluant	96	59	84
			Total	96	64	86
HMX	3	200	Eluant	88	56	66
			Total	89	87	73
		50	Eluant	87	51	59
			Total	87	62	68
	9	200	Eluant	91	74	83
			Total	93	105	90
		50	Eluant	80	64	80
			Total	80	79	89
DNT	3	200	Eluant	67	51	65
			Total	70	92	75
		50	Eluant	61	46	42
			Total	61	82	53
	9	200	Eluant	69	42	57
			Total	72	70	66
		50	Eluant	68	41	59
			Total	68	68	69
NG	3	200	Eluant	63	39	39
			Total	63	97	39
		50	Eluant	55	44	47
			Total	55	44	47
	9	200	Eluant	63	54	56
			Total	63	54	56
		50	Eluant	65	50	62
			Total	65	50	62

Values provided in percent recovered.

Table A6 — Soil Samples from Sites on Holloman Air Force Base

Sample ID	Site	Grid
HO-001	Old 2,000-lb crater	
HO-004	Old 2,000-lb crater	
HO-006	Old 500-lb crater	
HO-018	Low-order bomb crater	Hot
HO-019	Low-order bomb crater	Hot
HO-020	Low-order bomb crater	Hot
HO-022	2,000-lb crater	Hot
HO-023	2,000-lb crater	Hot
HO-024	2,000-lb crater	Hot
HO-025	No visible low-order debris	Cold
HO-026	No visible low-order debris	Cold
HO-027	No visible low-order debris	Cold

Table A7 — Analysis of Soil Samples Using EPA Method 8330B

Sample	HMX	RDX	TNB	DNB	TNT	2-ADNT	4-ADNT	2,4-DNT	DNA
HO-001	ND	ND	0.01	ND	0.14	0.03	0.04	0.01	ND
HO-004	ND	0.01	0.03	ND	0.05	0.02	0.02	ND	0.01
HO-006	ND	0.01	ND	ND	ND	0.10	ND	ND	ND
HO-018	ND	ND	0.01	ND	0.15	ND	0.04	ND	ND
HO-019	ND	ND	0.01	ND	0.54	0.04	0.01	ND	ND
HO-020	ND	ND	ND	ND	2.02	0.05	0.04	ND	ND
HO-022	ND	0.25	0.03	ND	12.50	0.11	0.11	ND	ND
HO-023	ND	0.04	0.03	ND	2.60	0.12	0.09	0.08	ND
HO-024	ND	0.01	0.01	ND	2.70	0.12	0.11	ND	ND
HO-025	ND	ND	0.08	ND	0.58	ND	ND	ND	ND
HO-026	0.01	ND	0.03	ND	0.19	0.06	ND	ND	0.01
HO-027	ND	0.02	0.02	ND	0.08	0.11	0.03	0.01	ND

Results provided by Cold Regions Research and Engineering Laboratory, Engineer Research and Development Center, U.S. Army Corps of Engineers.
ND denotes levels below the detection limit for the analytical method.
Concentrations are provided as parts per million (ppm) under the sample conditions applied in this study.
DNA = dinitroaniline.

Table A8 — Analysis of Soil Samples Using MM1 Sorbent Column

Target	Sample	HO-001	HO-004	HO-006	HO-018	HO-019	HO-020	HO-022	HO-023	HO-024	HO-025	HO-026	HO-027
2,4-DNT	Extracted	0.01	ND	ND	ND	ND	ND	ND	ND	ND	ND	ND	ND
	Effluent	ND	ND	ND	ND	ND	ND	ND	ND	ND	ND	ND	ND
	Eluate	0.33	ND	ND	ND	ND	0.06	ND	<0.01	ND	ND	ND	<0.01
2-ADNT	Extracted	0.01	ND	ND	ND	0.03	0.02	ND	ND	ND	ND	ND	ND
	Effluent	ND	ND	ND	ND	ND	ND	ND	ND	ND	ND	ND	ND
	Eluate	0.29	0.01	0.01	ND	0.43	0.50	0.09	0.08	0.07	0.02	0.01	0.01
4-ADNT	Extracted	0.02	ND	ND	<0.01	ND	ND	ND	ND	ND	ND	ND	ND
	Effluent	ND	ND	ND	ND	ND	ND	ND	ND	ND	ND	ND	ND
	Eluate	0.35	0.24	ND	0.92	0.50	0.63	0.09	0.01	0.03	ND	ND	ND
DNB	Extracted	ND	ND	ND	ND	ND	ND	ND	ND	ND	ND	ND	ND
	Effluent	ND	ND	ND	ND	ND	ND	ND	ND	ND	ND	ND	ND
	Eluate	ND	ND	ND	ND	ND	ND	ND	ND	ND	ND	ND	ND
HMX	Extracted	ND	ND	ND	ND	ND	ND	ND	ND	ND	ND	ND	ND
	Effluent	ND	ND	ND	ND	ND	ND	ND	ND	ND	ND	ND	ND
	Eluate	ND	ND	ND	ND	ND	ND	ND	ND	ND	ND	ND	ND
RDX	Extracted	1.32	<0.01	<0.01	ND	ND	ND	<0.01	ND	<0.01	ND	ND	<0.01
	Effluent	0.80	ND	ND	ND	ND	ND	ND	ND	ND	ND	ND	ND
	Eluate	5.23	0.07	0.07	ND	ND	ND	0.22	<0.01	<0.01	ND	ND	<0.01
TNB	Extracted	0.48	ND	ND	ND	ND	ND	ND	ND	ND	ND	ND	ND
	Effluent	0.21	ND	ND	ND	ND	ND	ND	ND	ND	ND	ND	ND
	Eluate	3.30	0.01	ND	<0.01	0.13	0.10	<0.01	<0.01	ND	ND	ND	ND
TNT	Extracted	6.59	0.29	ND	0.64	0.59	1.12	0.71	0.10	0.11	ND	ND	ND
	Effluent	1.73	<0.01	ND	0.04	ND	0.02	0.06	ND	ND	ND	ND	ND
	Eluate	54.59	2.87	ND	6.76	5.06	11.94	6.69	1.67	1.51	0.10	0.01	<0.01

Concentrations in parts per million (ppm). ND indicates not detected.

Table A9 — Comparison of MM1 and Commercial Sorbents on Soil Sample HO-022

Target	Method 8330B	NRL Extract		MM1	LiChrolut	Sep-Pak
2,4-DNT	ND	ND	Eluant	ND	ND	ND
			Total	ND	ND	ND
2-ADNT	110	16	Eluant	84	72	39
			Total	84	72	50
4-ADNT	110	68	Eluant	679	689	398
			Total	679	689	489
DNB	ND	ND	Eluant	ND	ND	ND
			Total	ND	ND	ND
HMX	ND	ND	Eluant	ND	ND	ND
			Total	ND	ND	ND
RDX	250	27	Eluant	127	36	21
			Total	127	36	45
TNB	30	8	Eluant	17	ND	ND
			Total	17	ND	ND
TNT	1250	386	Eluant	2950	2371	1798
			Total	2969	2814	2301

Concentrations in parts per million (ppm). ND indicates not detected.

Table A10 — Morphological Characteristics for Perchlorate Directed Sorbents

Material*	Surface Area (m^2/g)	Pore Volume (cm^3/g)	Pore Diameter $(Å)$	[Functional Group] $(mmol)^@$
HX Products				
HX	566	0.70	77	--
HX05M05B	342	0.43	64	1
HX2M	321	0.47	64	2
HX1M1B	206	0.29	63	2
HX4M	232	0.36	64	4
HX4B	342	0.34	63	4
HX2M2B	169	0.26	63	4
HX1M3B	163	0.22	53	4
HX2M4B	226	0.34	60	6
CF Products				
CF	523	0.57	111	--
CF05M05B	236	0.36	111	1
CF2M	197	0.29	93	2
CF1M1B	239	0.30	93	2
CF4M	25	0.04	111	4
CF4B	185	0.38	111	4
CF2M2B	143	0.18	93	4
CF1M3B	23	0.03	111	4
CF2	520	0.56	48	--
CF2-4M	108	0.12	38	6
CF3	562	0.52	64	--
CF3-4M	70	0.12	64	7

*Naming scheme uses base material followed by mmol quantity of alkylammonium group (B or M) used in grafting step.

@Total functional groups (TSPMC + TSPBC) applied per gram of sorbent during grafting step.

Table A11 — Summary of Ionic Targets Bound by NRL Variants and Commercial Materials

Material	Target Bound (µg)[#]					
	Perchlorate	Perrhenate	Nitrate	Thiocyanate	Sulfate	Phosphate
HX Products						
HX2M	239	333	114	166	311	200
HX1M3B	216	547	116	84	146	178
HX2M4B	54	330	68	20	121	164
CF Products						
CF4M	188	359	101	112	191	199
CF1M1B	339	633	158	180	78	168
CF2-4M	168	137	60	134	197	163
CF3-4M	258	257	91	191	250	191
Purolite Products						
A530E	670	1,000*	610	750	--	270
A532E	680	1,000*	760	750	--	270

[#]Sample used 10 mg of sorbent in a 200 ppm solution (5 mL).

*100% of target bound. When concentrations of targets were increased to 500 ppm, the Purolite resins also bound 100% of perrhenate (2510 µg), but only 1740 µg (A530E) and 650 µg (A532E) perchlorate.

Table A12 — Constants from Fits of Perchlorate Binding Isotherms

Material	K_P (M^{-1})	K_C (M^{-1})	X (mmol/g)
HX Products			
HX2M	662	494	1.86
HX1M1B	1428	985	1.92
HX4M	6380	881	0.45
HX2M2B	625	844	0.91
HX1M3B	1076	112	0.79
CF Products			
CF2M	1424	789	1.79
CF1M1B	2738	4359	1.85
CF4M	7550	741	0.28
CF4B	8984	265	0.56
CF2M2B	776	3102	1.46
CF1M3B	833	192	1.09
CF2-4M	2348	1104	0.81
CF3-4M	6719	3974	1.74

Table A13 — Perchlorate Preconcentration from Deionized Water

Target (ppm)	Effluent	Rinse 1	Eluent	Purge	Rinse 2	Total
0.2	0.0	0.1	6.6	2.8	0	9.6
0.5	2.1	0.3	15.9	8.0	0	26.3
1	4.7	0.5	30.5	12.0	0	47.6
2	13.4	1.1	62.1	24.1	0	100.7
5	52.9	3.7	148.6	46.4	0	252.0
10	5.30	0.1	72.4	9.6	0	506.0

Values are in μg

Table A14 — Perchlorate Preconcentration from Mixed Target Solutions

Target (ppm)	Effluent	Rinse 1	Eluent	Purge	Rinse 2	Total
2 ppm perchlorate +	33.1	1.8	38.7	5.1	0.0	78.8
2 ppm perrhenate	89.8	0.0	21.8	0.0	0.0	61.6
10 ppm perchlorate +	207.0	14.8	239.3	15.4	0.0	476.5
5 ppm perrhenate	107.7	7.4	97.5	4.6	1.6	218.6
5 ppm perchlorate +	9.6	6.4	115.7	6.8	0.0	228.7
10 ppm perrhenate	293.6	19.3	205.0	6.5	1.3	525.8
2 ppm perchlorate +	33.8	2.0	38.9	0.0	0.0	74.8
2 ppm thiocyanate	43.4	3.3	37.6	5.5	0.0	89.9
10 ppm perchlorate +	214.3	10.6	222.1	10.6	0.0	457.7
5 ppm thiocyanate	119.9	5.7	91.3	8.8	0.0	225.8
5 ppm perchlorate +	113.8	21.6	79.0	0.0	0.0	214.5
10 ppm thiocyanate	234.3	45.6	149.4	9.6	0.0	439.0

Values are in μg